AIAA 2000-3239

Blade Surface Pressure Distributions in a Rocket Engine Turbine: Experimental Work with On-Blade Pressure Transducers

Susan T. Hudson
Department of Mechanical Engineering
Mississippi State University
Starkville, MS

Thomas F. Zoladz and Lisa W. Griffin
Space Transportation Directorate
NASA Marshall Space Flight Center
Huntsville, AL

36th AIAA/ASME/SAE/ASEE
Joint Propulsion Conference and Exhibit
16-19 July 2000 / Huntsville, Alabama

AIAA 2000-3239

BLADE SURFACE PRESSURE DISTRIBUTIONS IN A ROCKET ENGINE TURBINE: EXPERIMENTAL WORK WITH ON-BLADE PRESSURE TRANSDUCERS

Susan T. Hudson*
Department of Mechanical Engineering
Mississippi State University
Starkville, MS 39762

Thomas F. Zoladz† and Lisa W. Griffin‡
Space Transportation Directorate
NASA Marshall Space Flight Center
Huntsville, AL 35812

Abstract

Understanding the unsteady aspects of turbine rotor flowfields is critical to successful future turbine designs. A technology program was conducted at NASA's Marshall Space Flight Center to increase the understanding of unsteady environments for rocket engine turbines. The experimental program involved instrumenting turbine rotor blades with surface-mounted high frequency response pressure transducers. The turbine model was then tested to measure the unsteady pressures on the rotor blades. The data obtained from the experimental program is unique in three respects. First, much more unsteady data was obtained (several minutes per set point) than has been possible in the past. Also, two independent unsteady data acquisition systems and fundamental signal processing approaches were used. Finally, an extensive steady performance database existed for the turbine model. This allowed an evaluation of the effect of the on-blade instrumentation on the turbine's performance. This unique data set, the lessons learned for acquiring this type of data, and the improvements made to the data analysis and prediction tools will contribute to future turbine programs such as those for reusable launch vehicles.

Nomenclature

C_0: Spouting Velocity (ft/s)
C_p: Specific heat at constant pressure (BTU/lb_m°R)
FP: Flow parameter
g_c: Conversion constant (32.174 (ft*lb_m)/(lb_f*s^2))
J: Conversion constant (778.3 ft-lb_f/BTU)
N: Speed (RPM)
N: Synchronous spectral component
P: Pressure (psia)
Pr: Pressure ratio
SP: Speed parameter
T: Temperature (°R)
Tq: Torque (ft-lb_f)
U: Disk tangential speed (ft/s)
U: Uncertainty
$\dot{W}$: Mass flow rate (lb_m/sec)
γ: Ratio of specific heats
η: Efficiency

Subscripts
0: Total
1: Inlet
2: Exit
ave: Average
Fac: Facility
th: Thermodynamic method
t-s: total-to-static
t-t: total-to-total

Introduction

The goals of next generation and future generation reusable launch systems are to increase safety and reliability, to reduce unit and/or operational costs (life, time between replacement and overhauls, operations complexity), and to reduce weight. To meet these goals, rocket engine

* Assistant Professor, Senior Member AIAA
† Aerospace Engineer
‡ Team Leader

components are required to be smaller, lighter weight, higher performing, more reliable, and less costly. These requirements push turbine designs to operate beyond the limits of the past. The flow through a turbine stage has always been extremely complicated. The rotor flowfield in particular is unsteady and generally three-dimensional. This flowfield unsteadiness is a major factor in turbine performance and life, and, as the turbine designs become more compact and closely coupled to meet new size and weight requirements, the flowfield unsteadiness increases. Therefore, understanding the unsteady aspects of the flowfield is critical to successful future turbine designs. This understanding will lead to designs in which unsteadiness is reduced or managed in order to provide more durable, higher performing turbines to meet program goals.

A technology program was conducted at NASA's Marshall Space Flight Center (MSFC) to increase the understanding of unsteady environments for rocket engine turbines. The program involved instrumenting the 1st stage rotor blades of the space shuttle main engine (SSME) high-pressure fuel turbopump (HPFTP) turbine with surface-mounted high frequency response pressure transducers. The HPFTP turbine model was then tested in air in the MSFC turbine test facility (TTE) to measure the unsteady pressures on the rotor blades. Simultaneously, a time-accurate computational fluid dynamics (CFD) code was being developed to allow accurate predictions of the unsteady environments yet requiring only a fraction of the computer time needed by unsteady codes of the past.

This paper discusses the experimental program. It describes the air test conducted in the TTE. It includes sections describing the test facility, the test model, and both the steady and unsteady instrumentation and data acquisition equipment. Issues critical to the success of the test, such as transducer calibration and data rates, are discussed. Steady turbine performance data is presented and compared with performance data obtained from a previous test of the model in the same configuration with no unsteady instrumentation. Blade surface pressure data is then presented to demonstrate data repeatability and validation. Finally, reduced time averaged and time resolved pressure data is discussed. This unique data set, the lessons learned for acquiring this type of data, and the improvements made to the data analysis and prediction tools will contribute to future turbine programs such as those for reusable launch vehicles. A comparison of this data set with the unsteady CFD code results will be the subject of a future article.

Facility Description

The test was conducted in the Marshall Space Flight Center's (MSFC) cold airflow Turbine Test Facility (TTE).[1] The TTE (Fig. 1) is a blowdown facility that operates by expanding high-pressure air (420 psig) from one or two 6000 cubic feet air tanks to atmospheric conditions. Air flows from the storage tanks through a heater section, quiet trim control valve, and a calibrated subsonic mass flow venturi. Flow then continues through the test model, backpressure valve, and exhausts to atmosphere. The facility can accommodate axial flow, radial inflow, and radial outflow turbines.

This equipment can deliver up to 220 psia air for run times from 30 seconds to over one hour, depending on inlet pressure and mass flow rate. The heater allows a blowdown-controlled temperature between 530° R and 830° R. The facility has manual set point closed-loop control of the model inlet total pressure, inlet total temperature, shaft rotational speed, and pressure ratio. In addition to these control parameters, the facility can accurately measure mass flow rate, torque, and horsepower. The associated data system is capable of measuring 512 pressures, 120 temperatures, and several model health-monitoring variables.

Model Description

The model tested, named the HPFTP Turbine Test Article (TTA), was a full-scale model of the Rocketdyne HPFTP turbine with rough rotor blades in the baseline configuration (Fig. 2). The model had been tested previously in this configuration, and the performance test results are documented in reference 2. As in the previous testing, the meanline airfoil diameter was 10.069 inches. The inlet struts, stators (or vanes), and rotors accurately duplicated the gas path geometry of the SSME HPFTP turbine. The turbine stages were actual engine hardware fitted and instrumented in the model casing. There were 13 inlet struts, 41 1st stage vanes, 63 1st stage rotor blades, 39 2nd stage vanes, and 59 2nd stage rotor blades. The model inlet flow was axially fed into the turbine with zero swirl. The exit guide vanes were located downstream of their engine position to allow room for instrumentation at the 2nd rotor exit. The SSME turbine exit circumferential pressure gradient was not simulated. The model exhausted into an axial annulus that lead to a collector. The collector directed the flow radially downward and diffused the flow to minimize the circumferential pressure gradient at the test article exit. The rotor tip and seal clearances represented the engine nominal clearances. The disk coolant flows and blade platform

seal leakages were not simulated. This test was designed to evaluate uncooled turbine performance; as such, all internal leakage paths were sealed, with the exception of small well-defined ventilating flows to prevent disk cavity heating. Unlike the previous testing, the model bullnose was modified for this test to accommodate a slip ring unit for the unsteady pressure measurements.[3] The effect of this modification on turbine performance will be addressed when the test results are presented.

Instrumentation

The TTA contained steady performance instrumentation as well as pressure transducers on the blades for the unsteady measurements. The steady instrumentation served two purposes: performance evaluation and model health monitoring. This instrumentation included pressures (total and static), temperatures, flow angles, shaft speed pickups, and accelerometers. An overview of the steady model instrumentation is given in Table 1. Reference 4 contains more details on the model instrumentation.

Table 1. Steady Instrumentation Overview

Turbine Inlet and Exit:
4 total pressure rakes (4 probes each at inlet and 5 probes each at exit).
4 total temperature rakes (4 probes each at inlet and 5 probes each at exit).
2 auto-nulling cobra probes with radial actuators.
Automatic circumferential traverse.
Turbine:
8 inner and 8 outer wall static pressures at 6 axial planes.
Stator surface static pressures—6 on pressure side and 8 on suction side at 10% span, 50% span, and 90% span on both stages.
14 stator outer shroud and 14 stator inner shroud static pressures on both stages.
Disk cavity static pressures.
Disk cavity total temperatures.
Exit Guide Vanes:
12 inner and 12 outer wall static pressures at 2 axial planes.
4 total pressure measurements on 6 vanes.
4 total temperature measurements on 6 vanes.
Miscellaneous:
2 speed pick-ups.
Accelerometers—2 horizontal, 2 vertical.
Contoured blank plugs for all bosses.
Health monitoring instrumentation.

The turbine inlet and exit planes were defined by instrumented rings. Each of the rings accommodated a total of eight rakes and two probes with radial actuators. Each rake contained four probes (total pressure or temperature) at the turbine inlet and five probes (total pressure and temperature) at the turbine exit. These rakes could be manually adjusted for yaw angle. The probes used with the radial actuators were three-hole cobra probes that were calibrated to obtain yaw angle, total pressure, static pressure, and total temperature. These cobra probes were used in the "auto-nulling" mode. The circumferential traverse actuators were not used on the inlet and exit rings. Both rings were "locked" in the 0° position.

The model included numerous static pressure measurements along the turbine inner (ID) and outer (OD) flowpath walls. Static pressure instrumentation was also present on the stator vanes along the suction and pressure surfaces at 10%, 50%, and 90% span. Rotor tip clearances were measured during the model build, but tip clearance probes were not used during testing since previous testing had shown that the tip clearance variation due to model test conditions over the complete test matrix was minimal.

The 1st stage turbine blades were instrumented with a total of 24 semiconductor type miniature fluctuating pressure transducers manufactured by Kulite.[3] The installed frequency response of the transducers was 100 kHz which provided ample bandwidth for the experiment since the 1st stationary vane passage frequency was approximately 4800 Hz. Fluctuating pressure transducer footprints were approximately 0.5 mm X 0.5 mm with the sensing diaphragm flush with the blade surface (Fig. 3). The sensors were distributed over seven turbine blades at various span and chord locations. Table 2 describes the sensor locations in detail.

Sensor wiring was routed down each blade across the disk to a wire carrier where a pin connection was made to a slip ring.[3] A 100 channel Litton Polyscientific gold surface high-speed slip ring unit (SRU) routed the sensor output to the downstream signal conditioning and data acquisition equipment. The model was modified to accommodate the SRU and a Hewlett-Packard shaft encoder. Since the model bullnose was modified to use the slip ring unit, the total pressure and total temperature rakes on the turbine inlet rotating ring were also modified from the previous performance testing. A spacer was used with these rakes to lift one of the sensors out of the flow; therefore, each inlet rake only had four probes radially in the flow in place of the five used on the previous test.

Table 2. On-Blade Instrumentation Locations

Blade #	% Span	% Axial Chord	% Wetted Length	Suction/ Pressure
21	90	14	12.5	P
21	90	58	47.6	P
21	90	75	65.5	P
22	90	7	8.5	S
22	90	22	19.1	S
22	90	88	81.3	S
42	10	13	12.0	P
42	10	59	49.6	P
42	10	77	66.2	P
43	10	5	8.3	S
43	10	18	20.0	S
43	10	60	51.0	S
43	10	83	74.7	S
63	50	10	9.4	P
63	50	23	20.3	P
63	50	52	44.1	P
63	50	82	75.0	P
1	50	5	7.3	S
2	50	9	11.5	S
1	50	19	19.0	S
2	50	25	24.0	S
1	50	61	50.1	S
2	50	72	61.9	S
1	50	89	83.0	S

High Frequency Data Acquisition

Banks of remotely controlled Pacific Instrument amplifiers were used to amplify the millivolt scale outputs of the on-blade pressure signatures. Two independent high frequency data acquisition systems were used concurrently in the experimental effort. The first utilized a collection of single-channel transient data recorders, also manufactured by Pacific Instruments. The system was capable of capturing at least 18 shaft revolutions. Both the amplifiers and digitizing banks were controlled via personal computer using a Lab View interface.

The second unsteady data acquisition system used in the effort provided real-time display and acquisition of all on-blade pressure channels as well as the shaft position encoder channels (both once-per-revolution and 500 pulse-per-revolution signatures). The 32 channel Computer Aided Dynamic Data Monitoring and Analysis System (CADDMAS) was developed as a cooperative research effort with Vanderbilt University, Arnold Engineering and Development Center, and Marshall Space Flight Center.[5,6] The CADDMAS is a parallel processor based on digital signal processors, analog/digital front-end processors, and standard personal computers. Using a parallel processing approach, the system achieves supercomputer performance in an interactive, high data-bandwidth environment.

The real-time capability of the CADDMAS to both display and acquire all of the on-blade measurements proved invaluable throughout the test series. Instantaneous waveform display aided pre-test sensor calibrations and identified errors in signal conditioning setup prior to test runs. With the system, turbine fluctuating pressures were sampled at 85 kHz over acquisition sessions lasting on the order of minutes.

Transducer sensitivities of the installed pressure sensors were provided with delivery of the instrumented disk. To ensure transducer calibration accuracy, complete end-to-end (i.e. from sensor diaphragm through digital representation) calibrations were performed at least twice each test day. Care had to be taken to guarantee that the instrumented blades had reached thermal stability during static step pressurizations before calibration voltages were obtained. A slight shift in the bias sensitivities in several of the channels over the duration of the testing was noted. Similar behavior was noted by Dunn and Haldeman in their characterization of the SSME fuel turbine.[7] The researchers attributed most of their long-term sensitivity drift to loss of protective RTV coating on the sensor diaphragms. The MSFC turbine model sensors utilized a similar RTV protection layer.

Test Conditions

Testing was done at a total of 17 set points. First, the turbine's aerodynamic design point from the previous performance test[2] was repeated. This set point is referred to as the "old design point." It corresponds to the SSME 104% rated power level (RPL) based on the Rocketdyne engine power balance model of the late 1980's. Second, the turbine conditions were set to match the operating condition in reference 7. This set point is referred to as the "Calspan set point." Two sets of off-design conditions were then run. First, the turbine was set to 65, 70, 80, 90, 100, 104, and 109% RPL based on the updated 1997 version of the Rocketdyne engine power balance model. Then, the turbine was run over a range of conditions to change the incidence angle on the 1st stage rotor blades. Incidence angle set points included 0, ±5, ±15, and ±25 degrees. Finally, a high turbine pressure ratio set point was run.

The set point parameters for the test were the turbine inlet total pressure, inlet total temperature, speed, and pressure ratio. Results presented here will only be for the old design point (ODP) and the Calspan set point (CSP). The old design point set point conditions were P_{01}=100 psia, T_{01}=550° R, N=6982 RPM, and $Pr_{t\text{-}t}$=1.47. The Calspan set point conditions were P_{01}=50 psia, T_{01}=550° R, N=6747 RPM, and $Pr_{t\text{-}t}$ =1.61. Data from the other set points is available from MSFC to those interested.

Test Results and Discussion

Steady Performance Results

Table 3 gives a summary of the steady test results for the old design point (ODP) and the Calspan set point (CSP). Data from three test runs done at different times during testing was combined to obtain the final numbers for each set point for the current test. Each test run consisted of 10 frames of steady data. A sufficient time interval was allowed between each frame of data so that the frames could be considered independent results. The inlet and exit total pressures and temperatures given in the table are averages of the rake measurements. The turbine inlet and exit static pressures are averages of the inner and outer diameter wall static pressure measurements at these planes.

The turbine's velocity ratio, speed parameter, flow parameter, and efficiency are given in Table 3 to define the overall performance. To achieve the proper units, the velocity ratio equation was

$$\frac{U}{C_0} = \frac{\frac{10.069 * N}{229.18}}{\sqrt{2 g_c J C_p T_{01}\left[1-\left(\frac{P_{02}}{P_{01}}\right)^{\frac{\gamma-1}{\gamma}}\right]}} \qquad (1)$$

The turbine speed parameter and flow parameter were defined as follows:

$$SP = \frac{N}{\sqrt{T_{01}}} \qquad (2)$$

$$FP = \frac{\dot{W}\sqrt{T_{01}}}{P_{01}} \qquad (3)$$

Note that these are "engineering" definitions for these parameters, and they are not truly nondimensional.

The thermodynamic method of determining turbine efficiency was used.[8,9] The temperature drop across the turbine was measured to determine the actual enthalpy change. For this "cold" air flow turbine testing where the temperature was relatively low, an ideal gas was assumed and γ and C_p were considered constant.

$$\eta_{th} = \frac{T_{01} - T_{02}}{T_{01}\left[1-\left(\frac{P_{02}}{P_{01}}\right)^{\frac{\gamma-1}{\gamma}}\right]} \qquad (4)$$

Table 3. Steady Performance Results

	Previous Test	Current Test	
	ODP	ODP	CSP
Facility Measurements			
$P_{0\ Fac}$		99.90	50.26
$T_{0\ Fac}$		548.00	548.16
N	7004.45	7005.98	6763.11
$\dot{W}$	13.98	14.37	7.73
Model Conditions			
P_{01}	99.47	99.89	50.24
T_{01}	547.64	545.71	545.90
P_1	99.30	99.65	50.11
P_{02}	67.67	67.94	31.29
T_{02}	498.65	497.17	488.53
P_2	66.34	66.66	30.43
Pressure Ratios			
t-t	1.47	1.47	1.61
t-s	1.50	1.50	1.65
Overall Performance			
U/C_0	0.37	0.37	0.33
SP	299.31	299.91	289.46
FP	3.29	3.36	3.59
η_{th}	0.857	0.853	0.831

A detailed posttest uncertainty analysis was completed for the current test using the methodology in reference 10. Estimates for the systematic and random components of the uncertainties of the measured variables are given in Table 4. The random component estimates were obtained directly from multiple test results based on a large sample assumption, and they include set point repeatability.

Table 4. Uncertainty Estimates of Measured Variables

	ODP Random	CSP Random	Systematic
$P_{0\ Fac}$	0.050 psi	0.017 psi	0.11 psi
$T_{0\ Fac}$	0.10° R	0.27° R	1.0 ° R
N	1.3 RPM	1.3 RPM	1.0 RPM
$\dot{W}$	0.0037 lb_m/s	0.010 lb_m/s	1% reading
P_{01}	0.037 psi	0.018 psi	0.11 psi
T_{01}	0.11° R	0.26° R	1.0 ° R
P_1	0.034 psi	0.021 psi	0.11 psi
P_{02}	0.057 psi	0.044 psi	0.11 psi
T_{02}	0.079° R	0.16° R	1.0 ° R
P_2	0.060 psi	0.042 psi	0.11 psi

Data at the old design point test condition was compared to data obtained from previous testing to evaluate the effect of the unsteady instrumentation on the turbine's performance. Static pressure drops through the turbine as well as overall performance parameters were studied.

Figure 4 gives the static pressure drops through the turbine for both the current test and the previous test.[2] The y axis in Fig. 4 is the average of the inner and outer wall static pressure measurements at each plane normalized by the static pressure at the turbine inlet. The x axis represents each axial station: 1 is the turbine inlet, 2 is the 1st stator inlet, 3 is the 1st stator exit, 4 is the 2nd stator inlet, 5 is the 2nd stator exit, 6 is the turbine exit, 7 is the EGV inlet, and 8 is the EGV exit. Figure 4 shows that there was no measurable difference in the static pressure drop through the turbine between the current and previous tests.

To compare overall performance, several parameters were studied. These parameters included facility set points as well as calculated performance parameters. The facility set points were P_{01}, T_{01}, N, and Pr; therefore, speed parameter was a set point. The calculated performance parameters that were used to compare the two data sets included the velocity ratio, flow parameter, and thermodynamic efficiency. The data from both the current test and the previous test is given in Table 3. Estimates for the random component of the uncertainty of the calculated values are given in Table 5 for the current test. The random component estimates were obtained directly from multiple test results based on a large sample assumption, and they include set point repeatability. Values for the previous test were similar.

Table 5. Random Component Uncertainty Estimates of Calculated Values

	ODP Random	CSP Random
Pr_{t-t}	0.0011	0.0023
Pr_{t-s}	0.0012	0.0024
U/C_0	0.0004	0.0005
SP	0.066	0.092
FP	0.0011	0.0078
η_{th}	0.0009	0.0008

Table 3 shows that the pressure ratios and the velocity ratios were the same for both tests. The speed parameter increased by 0.2% for the current test. This was due to a slight difference in the turbine inlet temperature set by the facility. The flow parameter increased by 2.4% for the current test. The subsonic venturi used to measure the mass flow rate in the TTE was recalibrated between tests. The application of the new calibration data caused a shift in the measured mass flow rate and the corresponding flow parameter.

The thermodynamic method of calculating turbine efficiency was used to compare between the two tests. The calculated thermodynamic efficiency was 85.7% for the previous test and 85.3% for the current test. This gives $\Delta\eta$=0.4%. The methodology in reference 11 was used to evaluate the difference in efficiency obtained from the two tests. The temperature measurements for both tests were made with the same thermocouples, wiring, hook-up, and data acquisition system. Similarly, the pressure measurements were made with the same instruments, hook-up, and data acquisition system. No factors were identified to change the systematic uncertainties of the measurements used to calculate the thermodynamic efficiency between the two tests. The random component of the uncertainty in the thermodynamic efficiency, including test-to-test variations, was 0.0014 or 0.14%. Therefore, the uncertainty in the difference in efficiency between the two tests was calculated to be 0.004 or 0.4%.[11] Since $\Delta\eta \pm U_{\Delta\eta}$ includes 0, the difference is insignificant.[11]

In summary, the data comparison showed no significant changes in turbine performance between the two tests. This leads to the conclusion that the installation of the unsteady instrumentation and the modification to the model bullnose did not have a measurable effect on the turbine's performance.

Unsteady Results

Signal Analysis

The current effort borrowed signal processing techniques proven in rotating machinery diagnostics to extract critical periodic content within the fluctuating pressure data. In the health monitoring of high-speed turbopump rolling element bearings and helicopter gear boxes, element passing and mesh components are enhanced using time domain averaging. Traditional time domain averaging, or synchronous time averaging, relies on a trigger pulse provided by a tachometer to synchronize the averaging process with the shaft rotational motion. This approach can only guarantee that the first point of each record in the ensemble average is synchronized to the rotor. Use of an optical encoder based sampling scheme guarantees rotor synchronization but is often not practical in the field.[12]

A recent novel method of rotary system signal enhancement developed for MSFC under the Small Business Innovative Research program provides superior noise reduction without encoder driven sampling. The technique, called the Phase Synchronized Enhancement Method (PSEM), discretizes a signal in a synchronous sense via use of the instantaneous frequency of rotor speed. PSEM transforms the underlying synchronous process that is varying about some center frequency into a purely discrete tone. Likewise, all synchronous related components in the signal become discrete, enhancing the diagnostic content of the signature. Both synchronous time averaging and PSEM were utilized in the post processing of the MSFC on-blade pressure data.

Figure 5 displays both a standard and PSEM power spectral density (PSD) plot of a single on-blade pressure channel over a frequency band in the vicinity of the 1st harmonic of the 1st vane passage (i.e., 82N, 9550 Hz). The standard PSD in the upper trace of the figure exhibits a speed variation that smears all synchronous related components in the fluctuating pressure spectrum. The variation was approximately 18 RPM peak-to-peak at a frequency of 0.19 Hz. At high harmonics of synchronous, the variation in turbine speed was appreciable (2.5% of mean frequency at 82N). The lower spectrum displays the PSEM enhanced spectrum. This enhancement is critical to the accurate mapping of the on-blade environment. PSEM processing preceded the characterization of pertinent spectral components (i.e. 1st vane and 2nd vane passing, inlet strut wake, etc.) versus span and chord. Use of the method was quite convenient in that superior noise reduction could be attained from uniformly sampled data. Moreover, costly imbedded optical encoders could now be left out of future test articles.

Blade Surface Pressure Mappings

Figures 6 through 9 summarize the distributions of the major unsteady components in the blade surface fluctuating pressures. Figure 6 demonstrates the data repeatability and validity. It displays the mean surface pressures normalized by the turbine inlet total pressure at 90% span for both the suction and pressure side locations with negative wetted length indicating the pressure side. The mean value estimates consider the whole revolution of the blade. No partitioning of the blade to 1st vane passing sequence (i.e. focusing on individual blade–vane sectors) has been applied. Data from two facility set points are displayed—the solid circles denote ODP and the solid diamonds denote CSP. The long run durations offered by the turbine test facility together with the acquisition capability of the real-time high-speed system allowed for extended averaging of the data. The current normalized data was averaged over a thirty second interval, or approximately 3,000 shaft revolutions. A prediction by Boyle[13] (solid line) and environments measured by Dunn and Haldeman[7] (open triangles) are also shown in Fig. 6. The data compares well with both prediction and prior SSME high-pressure fuel turbine characterization while offering more definition of the on-blade surface pressure environment with additional chord locations.

Figure 7 shows the normalized unsteady pressure envelope (Pmax – Pmin) experienced at a blade surface location over a complete shaft revolution. As with the average pressure distribution, current data (solid circles denote ODP and solid diamonds denote CSP) is shown along with both predictions and results of the earlier experimental effort by Calspan (open triangles). Detailed descriptions of the two unsteady environment predictions developed by Chen/Eastland (solid line) and McFarland (dashed line) are given in reference 7. The current unsteady envelope results compare well with the Chen/Eastland prediction. The lower prediction of McFarland did not include viscous wake effects.

As seen in Fig. 7, the largest monitored surface fluctuating pressures at 50% span were seen at mid-chord on the suction surface. In hindsight, additional pressure gages in this vicinity would have helped map this critical region. With the good agreement between experimental data and prediction evident in this effort, future blade instrumentation location guidance by time accurate CFD predictions seems warranted.

Figures 8 and 9 map the normalized intensities of the major spectral components that constitute the acquired unsteady blade surface pressures. All span and chord locations are shown versus wetted length for one baseline set point (ODP). The normalized intensities were developed using root-mean-square (RMS) amplitude of the respective component frequencies taken from PSEM processed spectra. Record length for the spectral estimates corresponded to approximately 3,000 shaft revolutions. For the vane passing (1^{st} and 2^{nd} stationary vane rows) components, the sum of both the fundamental and first harmonics were included in the RMS estimates (i.e., 39N, 78N, and 41N, 82N, respectively) to encompass most of the nonlinear features of the wavelets. Figure 8 allows a direct comparison of the dominant inlet vane wake with that of the more subtle second stationary vane row. As expected, peak 1^{st} vane response correlated well to the overall unsteady envelope (Pmax – Pmin) since it is the dominant response over all pressure locations. The figure also shows a gradual increase in the 2^{nd} vane response from leading to trailing edge. At the 50% span - 83% wetted length position, the 2^{nd} vane amplitude is close to that of the 1^{st} vane passing wake. Figure 9 maps the normalized synchronous and inlet strut passing responses (N and 13N, respectively) versus wetted length. Span and chordwise trends in these components are not easily discernible. At 50% span near the blade leading edge, synchronous content is comparable to the 1^{st} vane passage (Fig. 8).

Figure 10 displays the synchronous time averaged normalized fluctuating pressures for the 50% span – suction side locations over a complete shaft revolution. Pressure bias has been removed to enhance the waterfall effect of the unsteady traces. Averaging time and facility set point are consistent with Fig. 9 and 10. Waterfall format was chosen to convey wavelet phasing and amplitude simultaneously with increasing chordal depth into blade represented by the y-axis and increasing angular displacement of rotor (relative to key index) from left to right on the x-axis. The high frequency noise exhibited at all chord locations roughly three times per revolution is thought to be slip ring noise since the intensity of the noise did not scale with inlet total pressure and shows no chordal – temporal progression. The averaged waveforms display many intricacies of the blade stationary vane interactions over a complete shaft revolution. The waterfall provides an alternative summary to the spectral breakdown information contained in Fig. 7 through 9. The dominance of the inlet vane passing response at approximately mid-chord is reinforced as is the synchronous content nearer the blade leading edge. The mingled influences of the 1^{st} and 2^{nd} stationary vane passing components can be seen in the last chord-wise trace at 89% axial chord.

Summary and Conclusions

A technology program to increase the understanding of unsteady environments for rocket engine turbines was successfully completed. Steady measurements used to evaluate turbine performance as well as unsteady pressure measurements on the turbine rotor blades were obtained.

The steady measurements were used to define the turbine's performance at each set point. Additionally, the existence of a comprehensive steady data set on the turbine tested allowed a unique opportunity to evaluate the effect of the installation of the unsteady instrumentation on the turbine's performance. Data comparisons between the current test and a previous test of the same configuration with no unsteady instrumentation showed that the unsteady instrumentation and resulting hardware modifications did not affect the performance of the turbine. This data also demonstrated excellent facility repeatability, both run-to-run and test-to-test.

With the unsteady data, success in the acquisition and evaluation of complex high-speed turbine on-blade surface pressure environments was shown. The benefit of advanced high-speed digital signal acquisition and processing was demonstrated in the accurate mapping of the blade unsteady pressures. The high-fidelity flow features characterized in the successful effort will undoubtedly aid the advancement of CFD prediction tools. Lessons learned will be invaluable in the planning and implementation of similar blade mapping efforts for advanced turbines for the next generation and future generation reusable launch systems.

Acknowledgements

The authors would like to thank the many MSFC personnel who contributed to the success of the test. Also, the work of Bill Neighbors, formerly of MSFC, and Dr. Ted Bapty, of Vanderbilt University, in developing the two unsteady data acquisition systems is much appreciated.

References

[1]Bordelon, W.J. Jr., Kauffman, W.J. Jr., and Heaman, J.P., "The Marshall Space Flight Center

Turbine Test Equipment; Description and Performance," ASME 93-GT-380, 1993.

[2]Hudson, S.T., Gaddis, S.W., Johnson, P.D., and Boynton, J.L., "Cold Flow Testing of the Space Shuttle Main Engine High Pressure Fuel Turbine Model," AIAA 91-2503, 1991.

[3]Hudson, S.T., "Space Shuttle Main Engine High Pressure Fuel Turbine Blade Pressures (TTE0009) Pretest Report," NASA/MSFC Memo ED34-01-93, April 8, 1993.

[4]Bordelon, W.J. Jr., "Space Shuttle Main Engine High Pressure Fuel Turbopump Turbine Test Article Phase IA Pretest Report," NASA/MSFC Memo ED33-51-90, July 5, 1990.

[5]Bapty, T.A., "Model-Based Synthesis of Parallel Real-Time Systems," Ph.D. Dissertation, Vanderbilt University, December 1995.

[6]Abbott, B.A. and Bapty, T.A., "Experiences Using Model-Based Techniques for the Development of a Large Parallel Instrumentation System," Proc. Conf. Signal Processing Applications and Technology, Cambridge, MA, pp 573-582, 1992.

[7]Dunn, M.G. and Haldeman, C.W., "Summary of Time-Averaged and Phase-Resolved Pressure and Heat Flux Measurements on the First Stage Vane and Blade of the SSME Fuel-Side Turbine," NASA Earth to Orbit Conference, pp 516-524, 1994.

[8]Rodi, F., Varetti, M., and Tomat, R., "Low Pressure Turbine Testing," AGARD-CP-293, Presented at the 56th Symposium of the AGARD Propulsion and Energetics Panel, Turin, Italy, September 29-October 3, 1980.

[9]Hudson, S.T. and Coleman, H.W., "A Detailed Uncertainty Assessment of Methods used to Determine Turbine Efficiency," AIAA 98-2711, 1998.

[10]Coleman, H.W. and Steele, W.G., *Experimentation and Uncertainty Analysis for Engineers*, 2nd Edition, Wiley, New York, 1999.

[11]Kammeyer, M.E. and Rueger, M.L., "On the Classification of Errors: Systematic, Random, and Replication Level," AIAA 2000-2203, 2000.

[12]Jong J., Jones J., and Zoladz T., "Phase Synchronized Enhancement Method for Space Shuttle Main Engine Diagnostics," NASA Advanced Earth-to-Orbit Propulsion Technology, 1994.

[13]Boyle, R.J. and Giel, P.W., "Three-Dimensional Navier-Stokes Heat Transfer Predictions for Turbine Blade Rows," AIAA-92-3068, 1992.

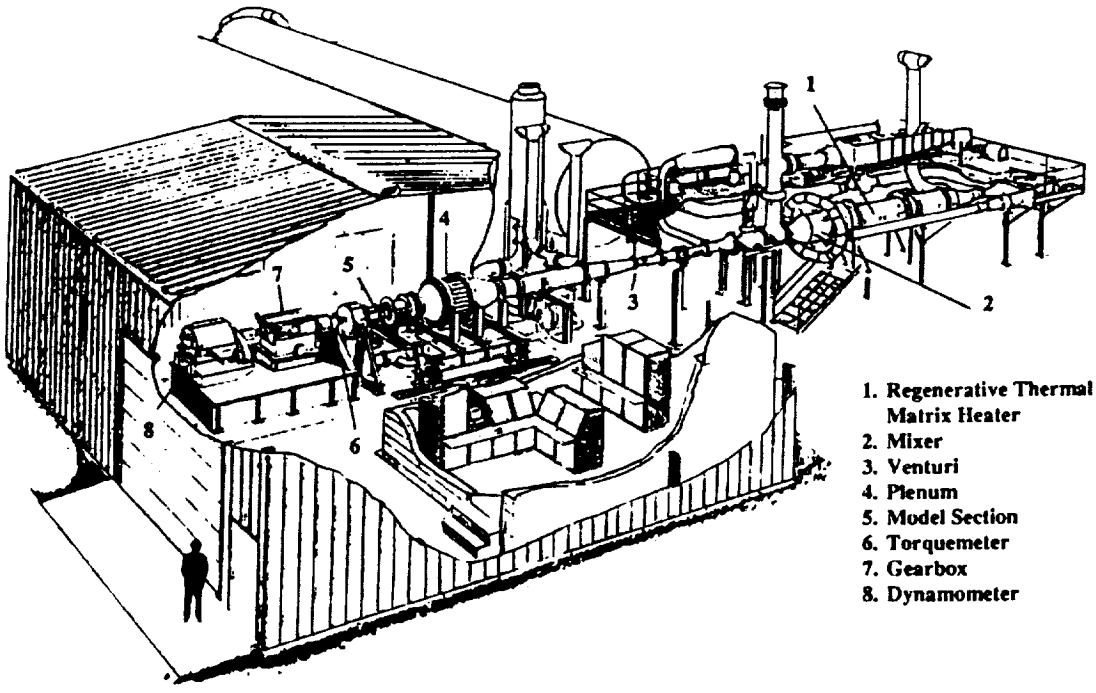

Fig. 1. Schematic of TTE

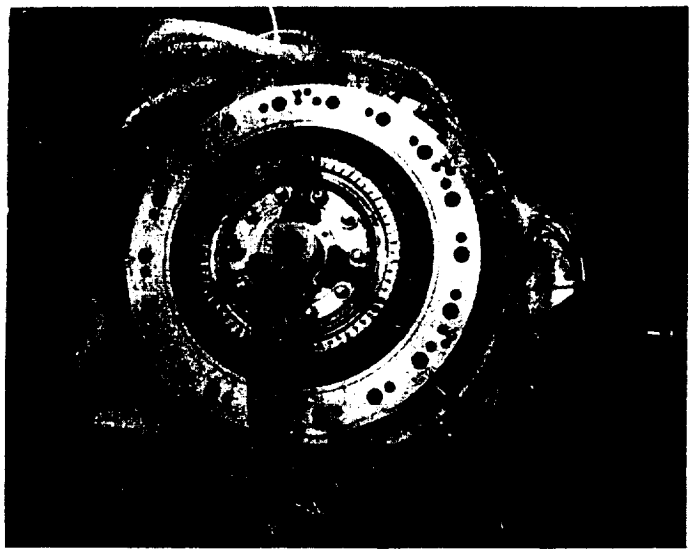

Fig. 2. Turbine Test Article

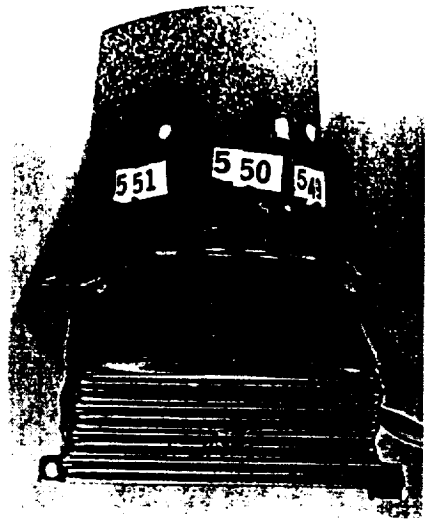

Fig. 3. Instrumented Blade (50% Span Suction Side)

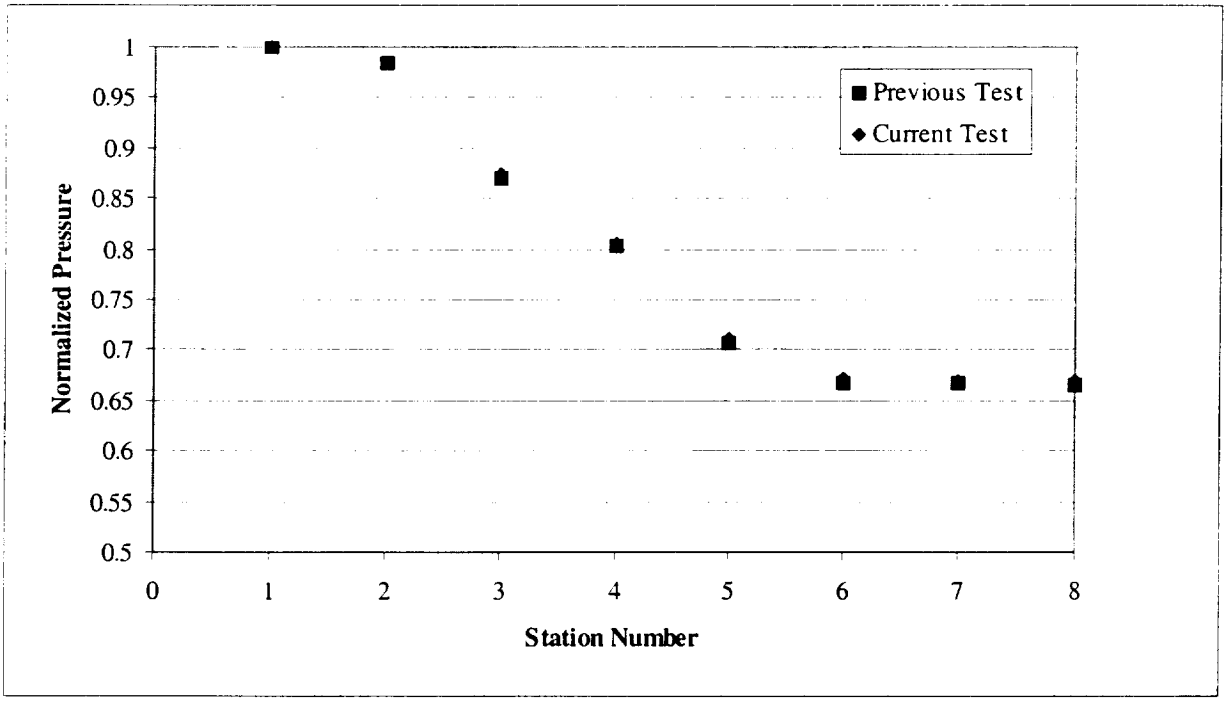

Fig. 4. Normalized Static Pressure Drop Through Turbine

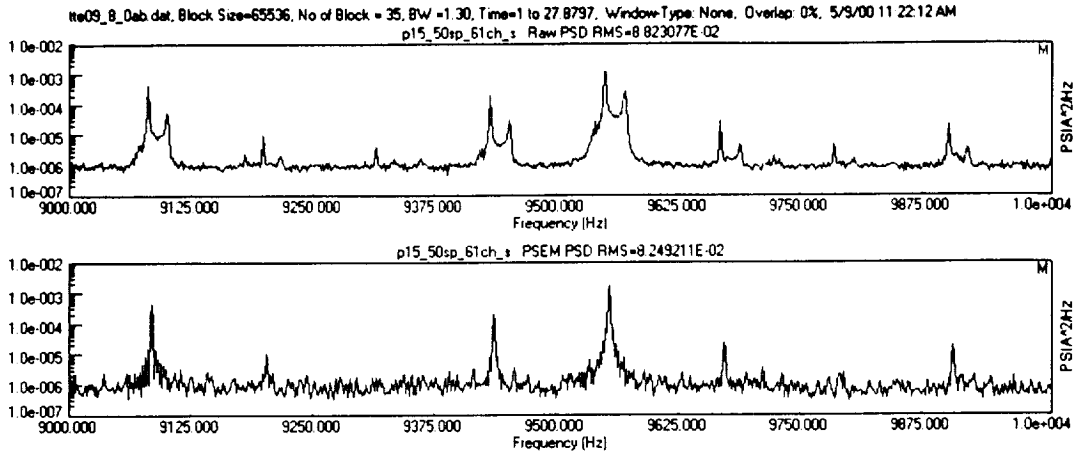

Fig. 5. Standard and Enhanced Pressures at 1st Harmonic of 1st Vane Passage Frequency

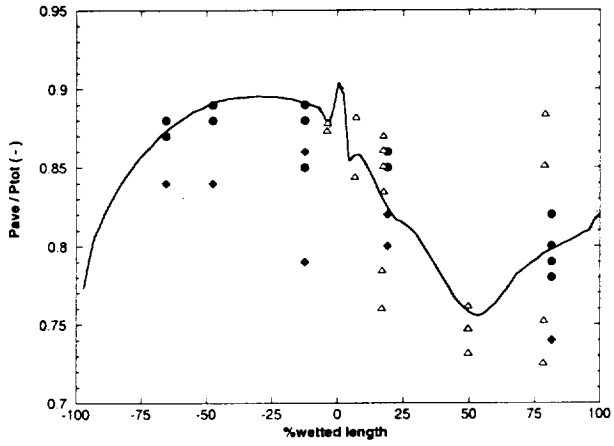

Fig. 6. 90% Span Normalized Average Pressure versus Wetted Length

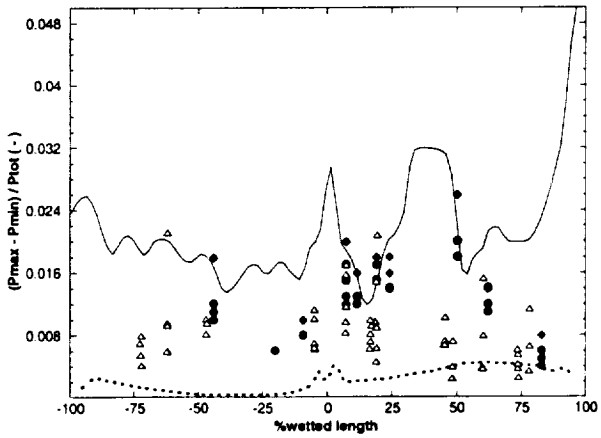

Fig. 7. 50% Span Normalized Pressure Envelope versus Wetted Length

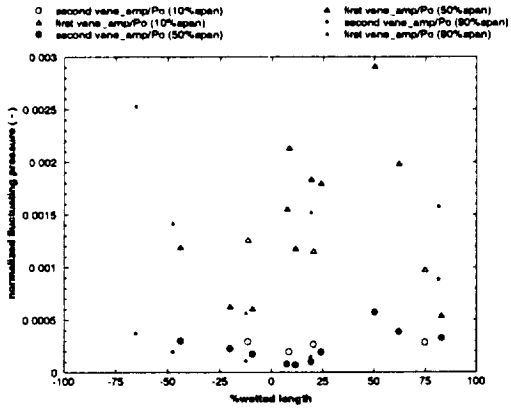

Fig. 8. Normalized Vane Passage Response versus Wetted Length

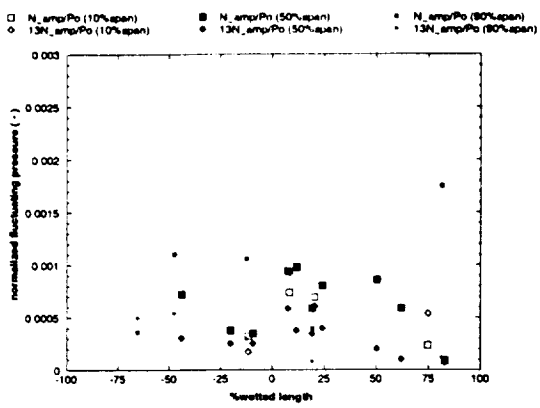

Fig. 9. Normalized Synchronous and Inlet Strut Passage Responses versus Wetted Length

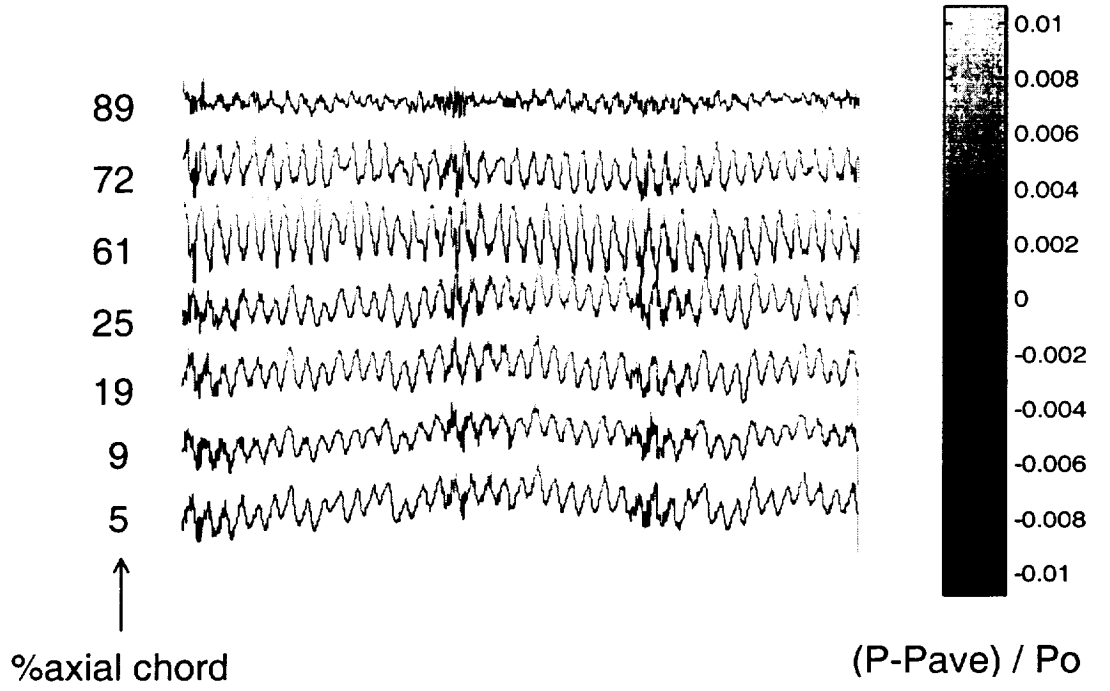

Fig. 10. Normalized Time Averaged Surface Pressures at 50% Span Suction Side